Original Article

JCBFM

Journal of Cerebral Blood Flow & Metabolism
2023, Vol. 43(2) 269–280

DOI: 10.1177/0271678X221129101
journals.sagepub.com/home/jcbfm
SAGE

Choroid plexus perfusion and bulk cerebrospinal fluid flow across the adult lifespan

Jarrod J Eisma[1], Colin D McKnight[2], Kilian Hett[1], Jason Elenberger[1], Alexander K Song[1], Adam J Stark[1], Daniel O Claassen[1] and Manus J Donahue[1,3]

Abstract

The choroid plexus (ChP) comprises a collection of modified ependymal cells that play an important role in the production of brain cerebrospinal fluid (CSF), and ChP perfusion aberrations have been implicated in a range of cerebrovascular and neurodegenerative disorders. To provide an exemplar for the growing interest in ChP activity, we evaluated ChP perfusion and bulk CSF flow cross-sectionally across the healthy adult lifespan. Participants ($n = 77$; age range = 21–86 years) were scanned at 3T using T_1-weighted, T_2-weighted-FLAIR, perfusion-weighted pCASL, and phase contrast MRI to calculate ChP anatomy, perfusion, and aqueductal CSF flow, respectively. Regression models were applied to evaluate aging effects on ChP volume and ChP perfusion in the lateral ventricles, as well as CSF flow. ChP volume (mean $\pm$ std $= 2.81 \pm 1.1$ cm^3) increased ($p < 0.001$), ChP perfusion (36.3 ± 8.6 mL/100 g/min) decreased ($p = 0.0078$), and ChP total blood flow (1.13 ± 0.34 mL/min) increased ($p < 0.001$) with age. Cranial-to-caudal net CSF flow (0.245 ± 0.20 mL/min) decreased, absolute CSF flow (4.86 ± 2.96 mL/min) increased, and CSF regurgitant fraction (0.87 ± 0.126) increased with age (all: $p < 0.001$). ChP perfusion was directly related to net cranial-to-caudal CSF flow through the aqueduct ($p = 0.033$). The implications of these findings are discussed in the context of the growing literature on CSF circulatory dysfunction in neurodegeneration and cerebrovascular disease.

Keywords

Aging, arterial spin labeling, cerebrospinal fluid, choroid plexus, glymphatic

Received 7 April 2022; Revised 28 July 2022; Accepted 4 September 2022

Introduction

The choroid plexus (ChP) comprises a highly vascularized collection of modified ependymal cells functioning at the interface of the blood-cerebrospinal fluid (CSF) barrier. Within the stroma of the ChP are fenestrated capillaries that passively filter plasma down the osmotic pressure gradient and across their endothelium into the stroma.[1] This filtrate is subsequently transported across the choroidal epithelium into the ventricular space, thereby releasing new CSF and metabolites into the CSF. While this process occurs in each of the brain's four ventricles at a rate of 430–530 mL/day,[2] most ChP tissue and associated CSF production is located in the atria of the lateral ventricles. The conventional view of CSF dynamics is that following CSF production in the lateral ventricles, arterial pulsations and pulmonary respiration direct CSF movement to the third ventricle through the foramen of Monro and then to the fourth ventricle through the aqueduct of Sylvius (i.e., cerebral aqueduct). At the fourth ventricle, CSF can enter the spinal subarachnoid space

[1]Department of Neurology, Vanderbilt University Medical Center, Nashville, TN, USA
[2]Department of Radiology and Radiological Sciences, Vanderbilt University Medical Center, Nashville, TN, USA
[3]Department of Psychiatry and Behavioral Sciences, Vanderbilt University Medical Center, Nashville, TN, USA

Corresponding author:
Manus J Donahue, Behavioral and Cognitive Neurology, 1500 21st Ave South, Village at Vanderbilt, Nashville, TN 37212, USA.
Email: mj.donahue@vumc.org

through the foramen of Magendie or the foramen of Lushka. Classically, CSF is understood to circulate along the brain and spinal cord prior to being resorbed into the venous system via the arachnoid granulations.[3]

The ChP has regained attention due to its possible relation to the newly hypothesized glial-lymphatic (i.e., *glymphatic*) waste clearance system of the brain.[4] The structure and function of the ChP and how it relates to CSF production could have important implications for neurodegenerative proteinopathies, which may have etiologies based in protein clearance and CSF production or circulation dysfunction.[4] A limitation to understanding these relationships derives from a general lack of methodologies for evaluating ChP activity and CSF flow non-invasively *in vivo* in humans.

To address this limitation, it is useful to note that the ChP receives its blood supply from the anterior and posterior choroidal arteries, which branch from the distal internal carotid arteries and P2 or P1 segments of the posterior cerebral arteries, respectively. These vessels arise from distal branches of arteries labeled frequently in pseudo-continuous arterial spin labeling (pCASL) MRI sequences. Recent work has shown that ASL methods can be re-parametrized to quantify ChP perfusion in the lateral ventricles[5,6] and blood-CSF water exchange,[7] partial volume correction or volume-corrected flow approaches can be applied,[8] and machine learning algorithms can be incorporated to accurately segment the ChP from the atria of the lateral ventricles using non-contrasted head anatomical images.[9] Using similar approaches, work from Johnson et al. found that ChP perfusion decreased after successful revascularization surgery in patients with Moyamoya vasculopathy, suggesting that ChP activity could be sensitive to circulating markers of ischemic stress or microvascular compliance.[5] Moreover, another study conducted by Alisch et al. found that ChP volume increases, ChP perfusion decreases, and ChP fractional anisotropy decreases with advancing age, which could reflect deteriorating structural integrity of the ChP with age.[10] This recent work highlights the feasibility and potential relevance of ChP perfusion imaging, however, understanding changes in ChP and CSF activity due to normal aging are required to disambiguate dysfunction due to aging from that which could be due to neurodegenerative or cerebrovascular disease.

We expand on these recent developments for ChP perfusion imaging and anatomical characterization by applying these methods in sequence with cardiac-synchronized phase contrast angiography of CSF flow through the aqueduct of Sylvius[11,12] in a larger cohort of healthy adults to understand how ChP perfusion, volumetry, and CSF aqueductal flow adjust across the lifespan and in relation to biological sex. Results are intended to for the first time characterize these relationships in healthy adults across the lifespan, which should serve as an exemplar for the growing work that seeks to investigate the role of CSF production and clearance dysfunction in neurodegenerative and cerebrovascular diseases.

Material and methods

Demographics and ethical considerations

Healthy, adult participants (n = 77) provided informed, written consent in accordance with the Vanderbilt University Institutional Review Board (IRB) and the Declaration of Helsinki and its amendments. All participants were enrolled between January 2020 and December 2021. Inclusion criteria for healthy control participants consisted of no history of cerebrovascular disease, anemia, psychosis, or neurological disorder including but not limited to prior overt stroke, sickle cell anemia, schizophrenia, bipolar disorder, Alzheimer's disease, Parkinson's disease, or multiple sclerosis. Presence of non-specific white matter lesions was not an exclusion criterion, as these lesions become more prevalent with aging, and we sought our cohort to be generalizable and representative.

Image acquisition

Images were collected on a Philips Ingenia system at 3 Tesla with body coil radiofrequency transmission and 32-channel SENSE-array reception (Philips Healthcare, Best, The Netherlands). Since it has been shown previously that CSF production activity is coupled to circadian rhythms,[13] we aimed to collect images at a consistent time of day between 7:00 AM and 11:00 AM. The anatomical images included for this study consisted of: (i) 3D T_1-weighted magnetization-prepared-rapid-gradient-echo (TR = 8.1 ms; TE = 3.7 ms; field of view = $256 \times 180 \times 150\,mm^3$; number of slices = 150; spatial resolution = $1.0 \times 1.0 \times 1.0\,mm^3$; duration = 4 minutes 32 seconds), (ii) 2D T_2-weighted fluid-attenuated-inversion-recovery (FLAIR) turbo-spin-echo (TR = 11,000 ms; TE = 120 ms; TI = 2800 ms; field of view = $230 \times 184 \times 144\,mm^3$; number of slices = 29; spatial resolution = $0.57 \times 0.57 \times 4.0\,mm^3$; duration = 1 minute 39 seconds), (iii) 3D T_2-weighted turbo-spin-echo (TR = 2500 ms; TE = 331 ms; field of view = $250 \times 250 \times 189\,mm^3$; number of slices = 242; spatial resolution = $0.78 \times 0.78 \times 0.78\,mm^3$; duration = 4 minutes 8 seconds), (iv) 2D diffusion-weighted spin-echo with single-shot echo-planar imaging readout (TR = 2926 ms; TE = 83 ms; field of view = $229 \times 229 \times 139\,mm^3$; number of slices = 28; spatial

resolution = $1.8 \times 1.8 \times 4.0\,mm^3$; b-value = $1000\,s/mm^2$; duration = 58 seconds), and (v) 3D time-of-flight magnetic resonance angiography (TR = 23 ms; TE = 3.5 ms; field of view = $200 \times 200 \times 84\,mm^3$; number of slices = 120; spatial resolution = $0.39 \times 0.39 \times 0.70\,mm^3$; duration = 4 minutes 7 seconds). These images and angiograms were used to ensure inclusion criteria were met.

Perfusion-weighted images were acquired using pCASL with dual background suppression pulses timed to null the longitudinal magnetization from gray and white matter, respectively, at the time of excitation. The blood vessels that supply the ChP, namely the anterior and posterior choroidal arteries, branch from the internal carotid and posterior cerebral arteries. The imaging volume was approximately centered on the corpus callosum, and we utilized a labeling offset of 100 mm, which equated to the labeling plane being placed approximately 30 mm below the base of the cerebellum. A train (duration = 1800 ms) of short (approximately 0.5 ms) Hanning-windowed radiofrequency pulses were used to label the inflowing blood in the internal carotid and vertebral arteries, and after a post-labeling delay of 2000 ms, 2D echoplanar imaging was utilized for readout (TR = 4550 ms; TE = 11 ms; field of view = $240 \times 240 \times 140\,mm^3$; number of slices = 20; spatial resolution = $3.0 \times 3.0 \times 7.0\,mm^3$; number of measurements = 30; duration = 4 minutes 42 seconds). The 2D approach was used rather than a 3D readout to reduce artifacts from signal smearing in the phase encode direction, as precise localization of the ChP was of interest in this study.

A phase contrast angiography (PCA) acquisition was adapted for use in the aqueduct of Sylvius to quantify CSF flow draining the lateral and third ventricles. Four MRI-compatible electrocardiogram (ECG) electrodes were placed on the chest and torso of the participant to allow for retrospective cardiac correction. The high spatial resolution 3D T_2-weighted scan described above was resliced on the scanner console in orthogonal planes and was used to plan the PCA acquisition slice orthogonal to the orientation of the aqueduct of Sylvius at the level of the tectum. A T_1-weighted, 2D gradient-echo scan (TR = 12.0 ms; TE = 7.8 ms; field of view = $150 \times 150 \times 4\,mm^3$; number of slices = 1; spatial resolution = $0.59 \times 0.59 \times 4.0\,mm^3$, duration = 5 minutes 10 seconds) was performed with the velocity encoding (VENC) value set to 12 cm/s and velocity encoding gradient direction set to foot-head. A velocity encoding value of 12 cm/s was utilized to minimize phase aliasing, obtain adequate signal, and prevent velocity overestimation near the perimeter of the aqueduct.[14]

Image analysis

Each participant's clinical history was reviewed by a board-certified neurologist (DOC; experience = 14 years), and anatomical imaging and angiography were reviewed by a board-certified neuroradiologist (CDM; experience = 12 years) to ensure that inclusion criteria were met.

For ChP segmentation, first the ChP in the atria of the lateral ventricles was segmented using anatomical images. The T_1-weighted and T_2-weighted FLAIR images were co-registered to $1\,mm^3$ isotropic MNI152 space using the Advanced Normalization Tools (ANTs) non-linear registration tools.[15,16] A deep learning model consisting of a fully convolutional neural network following the 3-D U-Net architecture was utilized to automatically segment the ChP in the atria and body of the lateral ventricles from these anatomical images.[9,17] Manual ChP segmentations from 30 participants were checked by the board-certified neuroradiologist (CDM) and used to train the neural network. The output segmentations were then back-transformed to the native T_1-weighted space, and from these masks the ChP volume and perfusion in the lateral ventricles were quantified. Representative segmentations from this method are shown in Figure 1.

For the calculation of ChP perfusion (mL/100 g/min), the source pCASL control and label images were surround subtracted,[18] slice delay corrected, equilibrium magnetization normalized, averaged, and then fit to a simplified general kinetic model[19] using the following parameters: blood-brain partition coefficient (λ) = 0.9 mL blood/g brain, labeling efficiency from the dual-background suppressed sequence (α) = 0.8, and the 3T $T_{1,blood} = 1.624$ s. The processed perfusion maps were co-registered to the T_1-weighted image using ANTs linear registration tools,[16] and the ChP segmentation from the machine learning model was applied to the perfusion maps to calculate the mean perfusion values in the ChP of the lateral ventricles. All perfusion maps in T_1 space were visually inspected for overlapping ChP perfusion-weighted signal and the ChP anatomical location in T_1 space by authors JJE, CDM, and MJD. A minimum threshold of 10 mL/100 g/min was used to ensure that all values were above the noise floor.[6] Mean gray matter perfusion was calculated by applying a gray matter mask produced from the ANTs Atropos tool to the T_1-registered perfusion maps using an identical noise threshold of 10 mL/100 g/min.[6,16] The total amount of blood supplied to the ChP (hereby named total blood flow; F) was calculated in units of mL/min using the following formula:[6]

$$F = \rho v N f \quad (1)$$

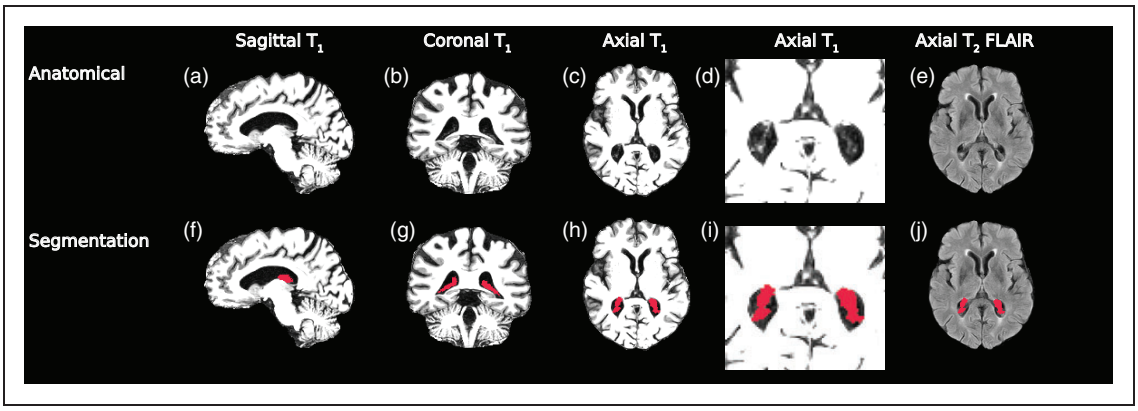

Figure 1. Anatomical images from a 71-year-old female were used for testing the deep learning model to segment the choroid plexus (a–d: T_1,: e:T_2-FLAIR). A 3-D U-Net architecture was employed to produce 3-D choroid plexus segmentations (f–j). T_1-weighted images have been windowed specifically to show contrast between choroid plexus and ventricles, rather than gray and white matter.

where ρ is the density of the choroid plexus in g/mL, v is the volume of each voxel in cm^3, N is the number of voxels labeled as choroid plexus, and f is the average perfusion of the ChP in mL/100 g/min. The mean density of the brain parenchyma (1.08 g/mL) was used to approximate the ChP density to maintain consistency with the mean brain-blood partition coefficient used in the perfusion quantification.

To calculate the bulk CSF flow parameters, the acquired PCA data were retrospectively cardiac phase-corrected (number of cardiac phases = 12) using the ECG trace collected during the acquisition. Local phase correction was applied during reconstruction of the PCA acquisition to reduce phase offsets from eddy currents and concomitant gradients. The aqueduct of Sylvius was manually delineated from the magnitude image (planned orthogonally to the aqueduct of Sylvius in the sagittal and coronal planes), and this mask was applied to the phase image from the PCA readout to obtain the acquired phase of the CSF flowing in the aqueduct of Sylvius throughout the cardiac cycle. The following formula was utilized for the calculation of flow velocity from the phase, assuming rectangular gradient waveforms:[20]

$$v = \frac{\Delta\phi}{2\gamma G\tau^2} \quad (2)$$

where v is the velocity of the moving spins in m/s, $\Delta\phi$ is the net phase difference (in radians) between the two images with alternating order of the bipolar phase-encoding gradients, γ is the gyromagnetic ratio of hydrogen protons (267.5 MHz · rad/T), G is the strength of the bipolar gradients (14.09 mT/m), and τ is the duration of one lobe of the bipolar gradient (1.41 ms). Mean volumetric flow (mL/s) was calculated as the product of the mean velocity (cm/s) and cross-sectional area of the aqueduct of Sylvius mask (cm^2). Next, the calculated velocity was multiplied by −1 to assign positive velocity and flow values to the caudal direction and negative velocity and flow values to the cranial direction. The mean volumetric flow (mL/s) of CSF through the aqueduct of Sylvius was calculated during each of the 12 prescribed phases of the cardiac cycle. A phase aliasing correction was included in the processing pipeline to correct the phase values from the few participants whose flow velocities exceeded the VENC value of 12 cm/s.

These 12 flow values then were fitted to a 6th order polynomial to smooth the data and account for any small variability in the data between the 12 sampling epochs. The net CSF flow (mL/min) and absolute CSF flow (mL/min) were calculated by integrating the raw and absolute value CSF flow curves across time, respectively (Figure 2), and multiplying these values by the participant's mean heart rate during the acquisition. We chose to standardize these values by the mean heartbeat to account for the variation in duration of each participant's cardiac cycle and to standardize these values on the same time scale as the perfusion measurements for statistical comparison. The net CSF flow represents the net volume of CSF that passes through the aqueduct of Sylvius within one minute, and the absolute CSF flow represents the total volume of CSF that passes through the aqueduct of Sylvius in either the cranial or caudal direction within one minute. The regurgitant fraction was calculated by dividing the negative area under the CSF flow curve by the positive area under the CSF flow curve, which represents the CSF volume that traveled in the

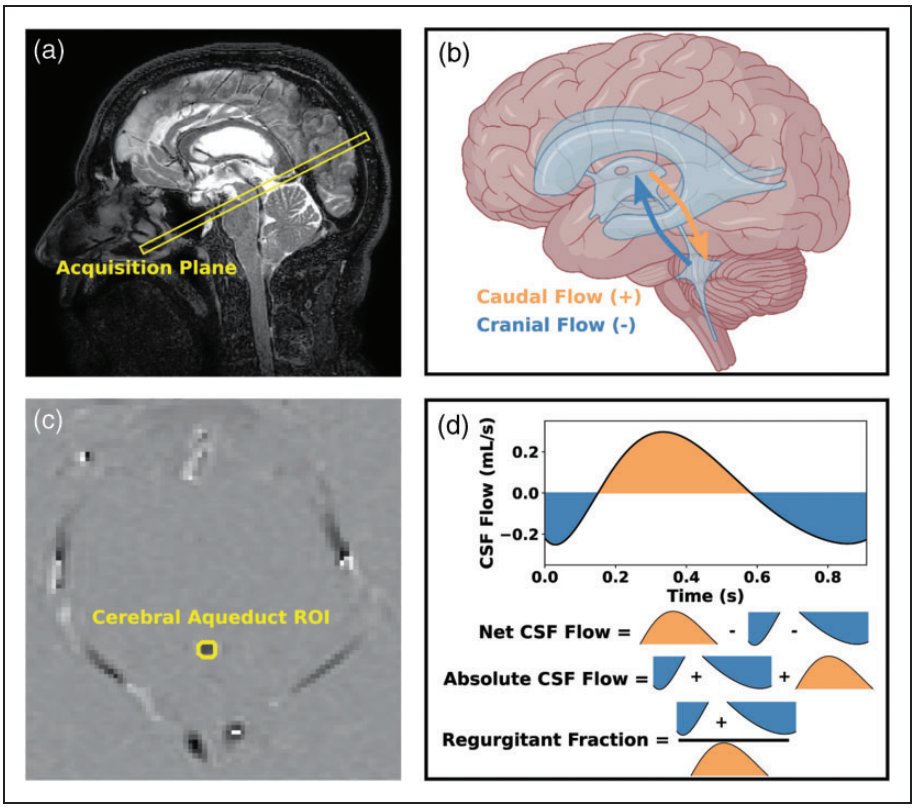

Figure 2. Overview of phase contrast acquisition. The imaging slice was planned orthogonal to the cerebral aqueduct of Sylvius (a: sagittal T_2-weighted image at midline). The direction of the bipolar, velocity sensitizing gradients was set to foot-head, but post-processing methods designated caudal flow with positive phase (b: orange) and cranial flow with negative phase (b: blue). A mask was drawn around the aqueduct of Sylvius to extract the phase values from that region (c: subtracted phase image), and these phase values were used to generate cerebrospinal fluid (CSF) flow curves and calculate the following metrics: net CSF flow, absolute CSF flow, and regurgitant fraction (d). Example data are shown from a 66-year-old male. (ROI: region of interest; CSF: cerebrospinal fluid; HR: heart rate).

cranial direction as a fraction of the CSF volume that traveled in the caudal direction within one minute.

Figure 2 illustrates the placement of the PCA slice and the axial phase image which were used for calculating the cardiac-corrected and phase-aliased corrected CSF flow measurements. The schematic shows the directionality and sign convention used for the study, as well as graphical representations of the net CSF flow, absolute CSF flow, and regurgitant fraction metrics. Note that in this analysis, cranial-to-caudal flow down the aqueduct is defined as positive CSF flow, and as such more positive net CSF flow across the cardiac cycle is consistent with higher CSF flow out of the lateral ventricles.

Statistical analyses and hypothesis testing

All statistical analyses were implemented using the R software package.[21] All p-values were corrected with false discovery rate multiple comparisons correction.[22] All data distributions were tested for normality using the Shapiro-Wilk test.[23] To test the hypothesis that the ChP hypertrophies with age, we applied separate generalized linear models with ChP volume (cm^3), perfusion (mL/100 g/min), and total blood flow (mL/min) as dependent variables and age and sex as independent variables (Wald-test significance criteria: $p < 0.05$). To test the hypothesis that CSF flow through the aqueduct of Sylvius changes with age, we applied separate generalized linear models with net CSF flow, absolute CSF flow, and CSF regurgitant fraction as dependent variables and age and sex as independent variables (Wald-test significance criteria: $p < 0.05$). Finally, to test the hypothesis that ChP perfusion is related to net CSF flow, we applied a generalized linear model with net CSF flow as the dependent variable and ChP perfusion and sex as independent variables (Wald-test significance criteria: $p < 0.05$). Exploratory analyses were conducted regressing ChP perfusion against absolute CSF flow, ChP total blood flow against net CSF flow, and ChP total blood flow against absolute CSF flow and these findings are presented in the supplementary materials.

Results

Participants (n = 77) ranged in age from 21 to 86 years and were comprised of 35 males and 42 females. All participants met neurological and radiological inclusion criteria as stated above. Demographic information for all participants is summarized in Table 1.

Table 1. Demographic information and summary statistics for subjects included in this study.

Sample size (n)	77
Age (years)	47.8 ± 18.2
Sex (M/F)	35/42
ChP volume (cm^3)	2.81 ± 1.06
GM perfusion (mL/100 g/min)	49.5 ± 6.1
ChP perfusion (mL/100 g/min)	36.3 ± 8.6
ChP total blood flow (mL/min)	1.01 ± 0.31
Net CSF flow (mL/min)	0.245 ± 0.198
Absolute CSF flow (mL/min)	4.86 ± 2.96
Regurgitant fraction	0.87 ± 0.126

Values are reported as mean ± standard deviation where applicable. FDR: false discovery rate; ChP: choroid plexus; GM: gray matter; CSF: cerebrospinal fluid.

Numerical results from all regression analyses are shown in Table S1. All p-values are reported after multiple comparisons correction unless noted otherwise. Figure 3 shows representative T_1-weighted and pCASL images from younger (age = 36 years) and older (age = 71 years) female participants. Scatter plots summarizing the ChP regression analyses are shown in Figure 4. Age was observed to be positively related to ChP volume ($p < 0.001$). Sex had a significant effect on the ChP volume, with males having larger ChP volumes compared to females ($p < 0.001$). Age was inversely related to the ChP perfusion ($p < 0.001$). Sex had a significant effect on ChP perfusion, with males having lower ChP perfusion compared to females, but only before multiple comparisons correction ($p = 0.038$). Age was positively related to the ChP total blood flow ($p < 0.001$). Sex had no significant effect on the ChP total blood flow ($p = 0.23$).

Scatter plots summarizing the CSF flow regression analyses are shown in Figure 4. It was observed that with increasing age, the net flow through the aqueduct

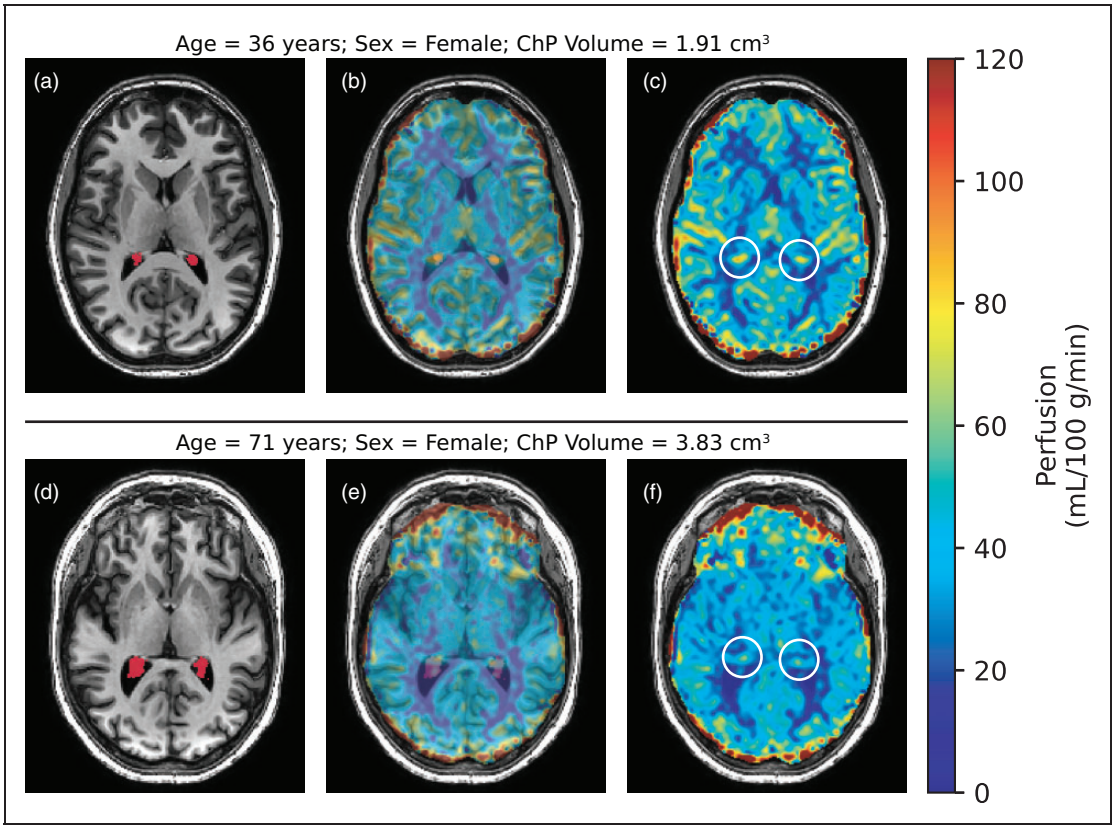

Figure 3. Choroid plexus (ChP) perfusion-weighted images were produced from pseudo-continuous arterial spin labeling. A 36-year-old, female (a–c) is compared to a 71-year-old, female (d–f). Smaller ChP volume (a: red segment) corresponds with increased perfusion (c: white circle), whereas enlarged ChP volume (d: red segment) corresponds with reduced perfusion (f: white circle). The middle column is included to show adequate co-registration between the perfusion-weighted and T_1-weighted images. (ChP: choroid plexus).

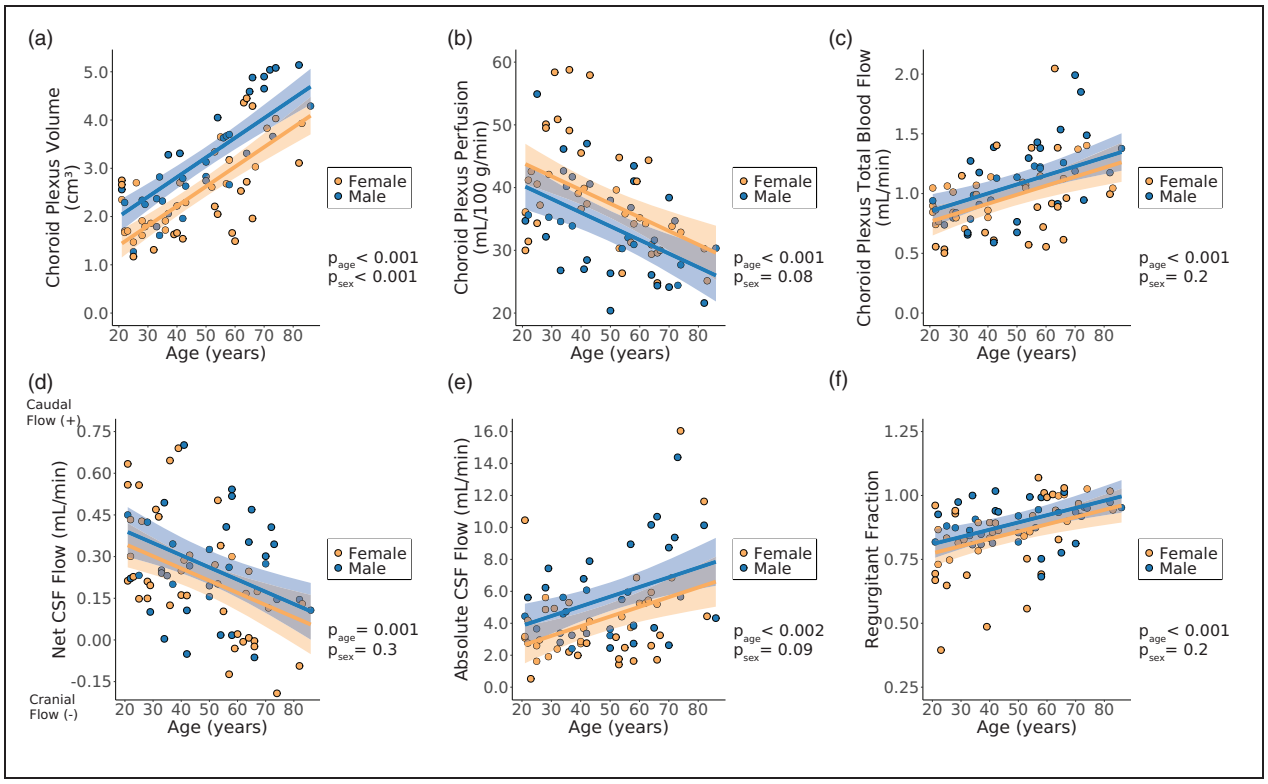

Figure 4. Results from choroid plexus regression analyses with volume (a), perfusion (b), and total blood flow (c) as the response variable and cerebrospinal fluid (CSF) regression analyses with net CSF flow (d), absolute CSF flow (e), and regurgitant fraction (f) as the response variable (Wald test significance criteria: $p < 0.05$). Generalized linear models were implemented with age and sex as explanatory variables. Shaded regions represent the 95% confidence interval for the fitted data based on the standard error of the prediction. All p-values shown were corrected for multiple comparisons. (CSF: cerebrospinal fluid; p_{age}: p-value for age coefficient in generalized linear model; p_{sex}: p-value for sex coefficient in generalized linear model).

of Sylvius decreases ($p = 0.0011$). Sex was not significantly related to the net CSF flow ($p = 0.28$). Age was positively related to the absolute CSF flow through the aqueduct of Sylvius ($p = 0.0019$). Sex had a significant effect on the absolute CSF flow, but only before multiple comparisons correction ($p = 0.049$), and age was positively related to the regurgitant fraction of CSF flow through the aqueduct of Sylvius ($p = <0.001$). Sex had no significant effect on the regurgitant fraction ($p = 0.22$). The interpolated CSF flow curves for all subjects included in this study are shown in Figure 5.

ChP perfusion increased with increasing net CSF flow. This finding was significant before, but not after, multiple comparisons correction ($p = 0.033$; Figure 6). ChP perfusion had no significant effect on the absolute CSF flow through the aqueduct of Sylvius ($p = 0.17$; Figure S1a). The ChP total blood flow had no significant effect on the net CSF flow through the aqueduct of Sylvius ($p = 0.40$; Figure S1b). The ChP total blood flow had a positive effect on the absolute CSF flow through the aqueduct of Sylvius ($p = 0.039$; Figure S1c), meaning that as the total blood delivered to the ChP increased, the total amount of CSF flowing through the aqueduct in either direction also increased.

Discussion

The purpose of this study was to apply noninvasive magnetic resonance imaging methods to quantify changes in the ChP anatomy and function, and to evaluate any variation in these metrics in relation to CSF aqueductal flow cross-sectionally across the healthy adult lifespan. The primary findings are that ChP in the atria of the lateral ventricles hypertrophies with age, ChP perfusion decreases with age, and that ChP total blood flow increases with age. Additionally, CSF flow becomes more regurgitant through the aqueduct of Sylvius with age, and net CSF flow through the aqueduct of Sylvius (cranial to caudal direction) tends to increase as ChP perfusion increases. This latter finding met significance criteria before, but not after, multiple comparison corrections.

Our finding that ChP volume increases with age has been reported previously in rats,[24] mice,[25] and, more

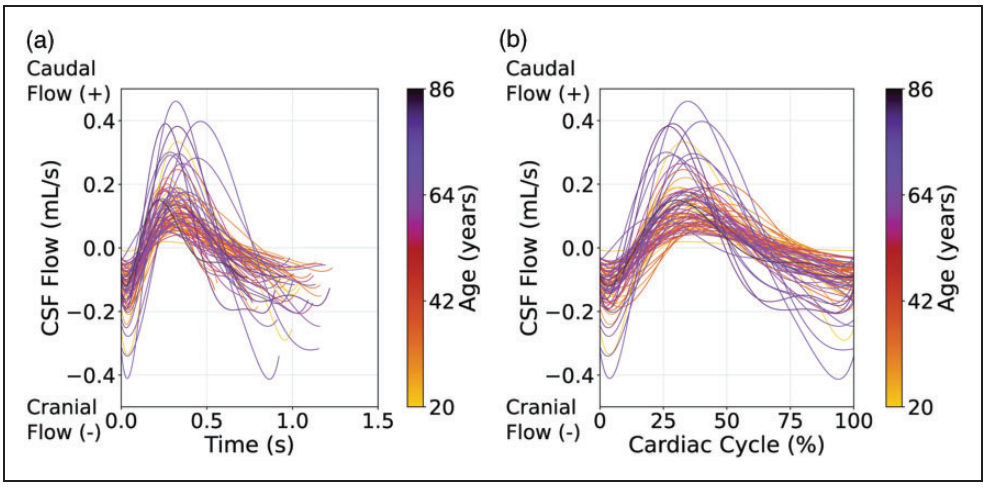

Figure 5. Cerebrospinal fluid (CSF) flow results. CSF flow curves for all participants, color-coded by age, are shown, with time of the cardiac cycle (a) and fraction of the cardiac cycle (b) displayed on the x-axes. As the age of participants increased, the peak-to-peak difference in the CSF flow curves increased. With increasing age, net CSF flow decreases, absolute CSF flow increases, and regurgitant fraction increases. (CSF: cerebrospinal fluid).

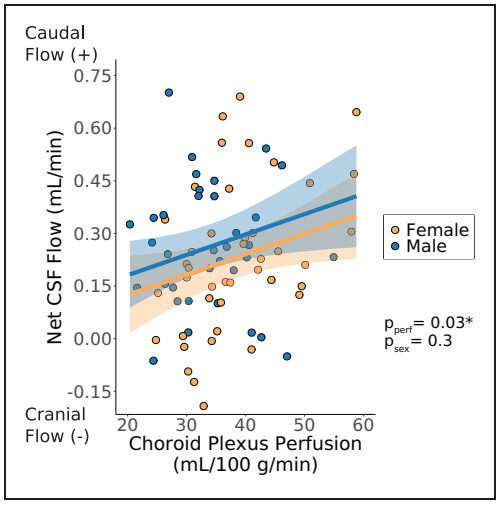

Figure 6. Net cerebrospinal fluid (CSF) flow versus choroid plexus perfusion; choroid plexus perfusion and sex are considered as explanatory variables (Wald test significance criteria: $p < 0.05$). Shaded regions represent the 95% confidence interval for the fitted data based on the standard error of the predictions. All p-values shown were corrected for multiple comparisons correction unless noted otherwise. * Signifies that the p-value for the choroid plexus perfusion coefficient was statistically significant before but not after multiple comparisons correction. (CSF: cerebrospinal fluid; p_{perf}: p-value for choroid plexus perfusion coefficient in generalized linear model; p_{sex}: p-value for sex coefficient in generalized linear model).

recently, humans;[10] as such, these findings when taken in isolation are largely confirmatory. Alisch and colleagues reported increases in ChP volume as a fraction of total intracranial volume with age.[10] Despite the differences in ChP segmentation algorithms between Alisch et al. and our study, the trend of increasing ChP volume with age remains consistent. We observed a significant effect of sex on ChP volume, a finding not observed in the study by Alisch et al., which may be explained by their choice to normalize ChP volume by total intracranial volume. Insight regarding this observed increase in ChP volume may come from post-mortem analyses of the human ChP, whereby increased thickening of the basement membrane of choroidal epithelial cells,[26] calcifications in the stroma of the ChP,[27] and thickening of the tunica media and adventitia in the arterial wall with increased age[28] have all been observed. The volumetric findings observed here are consistent with these previous post-mortem histological analyses.

Previous studies examined functional changes of the ChP with age in rats, finding that enzymatic activity decreased[29–31] and transport protein activity decreased[31,32] with increasing age. These findings, as well as our finding that ChP perfusion decreases with age, are consistent with the notion that choroidal CSF production decreases with age, which has been shown in anesthetized sheep[33] and verified in humans once, albeit using the often disputed Masserman method.[34] The decrease in ChP perfusion with age is also consistent with the findings from Alisch and colleagues, who reported a nonlinearly decreasing perfusion in the ChP with age using pCASL MRI methods. The observed increase in ChP volume that coincides with decreased ChP perfusion with advancing age may act as a compensatory mechanism to maintain sufficient aqueductal CSF flow.

We also investigated the relationship between ChP total blood flow and age. ChP total blood flow may be

a more comprehensive metric of ChP activity since it is less susceptible to partial volumes effect[6] and the mass of the ChP is smaller than the 100 gram normalization included in the perfusion calculation. We found that the total blood flow of the ChP increased with age, but, given that the volume of the ChP also increased with age, this finding perhaps is not surprising. We hypothesize that the total blood flow increase may be a compensatory mechanism of the blood-CSF barrier that occurs in response to the morphological changes of the ChP with aging. As ChP function declines with age, more blood may be delivered to the ChP to maintain sufficient CSF production for general CNS metabolism. It is worth noting that the increase in blood delivery may also serve to activate other functions of the ChP, such as secretion of ions, cytokines, growth factors and reabsorption of brain metabolites.

The findings that net caudal CSF flow through the aqueduct decreases, absolute CSF flow increases, and CSF regurgitant fraction increases with age, all support the view that aqueductal CSF flow becomes more dynamic with age. These changes in CSF flow dynamics are visualized in Figure 5. Previous work has analyzed aqueductal CSF dynamic changes due to aging in humans but with conflicting results.[35–38] Early work from Barkhof and colleagues found no effects of age on aqueductal CSF flow, but these findings are limited by the small sample size (11 young controls, 9 old controls) and the strength of the magnet used (0.6 T).[38] Work from Gideon et al. found no statistically significant difference in aqueductal CSF peak flow volume nor velocity in both the caudal and rostral directions between a group of healthy elderly participants ($n = 5$) and a group of healthy young participants ($n = 8$).[36] The velocity-sensitizing imaging method used in their study differed from ours and was implemented on a 1.5 T scanner. These factors, as well as the small sample size, limit the reproducibility of these findings. Work from Stoquart-ElSankari et al. found that aqueductal CSF stroke volumes decreased in a cohort ($n = 12$) of normal elderly subjects compared to a cohort ($n = 19$) of normal young subjects,[37] consistent with the finding in our study that net CSF flow through the aqueduct decreases with increased age. The major drawback from these early CSF dynamic studies is the limited sample sizes.

More recently, however, in a larger cohort of 128 healthy participants with an age range of 17 to 88 years, Sartoretti et al. observed that CSF stroke volume, forward (caudal) flow volume, backward (cranial) flow volume, and absolute stroke volume increased significantly with age.[35] We report that absolute CSF flow increases with increasing age and that there is a sex difference in absolute CSF flow, consistent with the findings reported by Sartoretti and colleagues. However, Sartoretti and colleagues found that net CSF flow through the aqueduct increases with increasing age and that age has an inconclusive effect on the regurgitant fraction of CSF flow through the aqueduct of Sylvius, which conflicts with our finding that the net CSF flow through the aqueduct decreases and regurgitant fraction increases with increased age. Discrepancies in these findings might be explained by differences in acquisitional parameters, the use of a peripheral pulse triggering unit for retrospective cardiac correction, and some ambiguities in the sign convention of the net flow direction described by Sartoretti et al. The data presented in our study were collected in a large cohort of healthy adults across the lifespan with an appropriate velocity encoding value of 12 cm/s and are unaltered aside from the interpolation method used to account for sampling aliasing.

This is the first study to show, using noninvasive MRI methods, that ChP perfusion in the lateral ventricles is directly related to CSF flow through the aqueduct of Sylvius. We evaluated ChP perfusion measured via pCASL MRI and aqueductal CSF flow measured via phase-contrast MRI to understand whether ChP perfusion provided a surrogate marker of choroidal CSF production. We observed that as ChP perfusion increased, the net CSF flow through the aqueduct increased in magnitude in the positive, caudal direction. Further, we found that ChP total blood flow, a metric less susceptible to partial volumes effects than average perfusion, was positively related to absolute CSF flow through the aqueduct of Sylvius. In other words, as more blood was delivered to the ChP, more CSF flow was observed through the aqueduct of Sylvius in either the cranial or caudal direction. Together, these findings provide support that ChP perfusion in the lateral ventricles is related to downstream CSF flow at the level of the aqueduct of Sylvius in healthy adults.

Previous studies in animals have attempted to quantify choroidal CSF production,[39,40] but the methods implemented introduced unphysiological variables related to changes in intracranial pressures from invasive procedures, and therefore it is unknown how well these findings translate to humans. The finding that choroidal CSF production might be detected using noninvasive MRI methods is novel and potentially lays a framework for quantifying CSF production in humans across all ages. However, there are caveats to this study. First, there is CSF flowing in the aqueduct of Sylvius that is extrachoroidal in origin and our methods lack the ability to distinguish alternative sites of CSF production. Supplementary analyses found that total brain CSF volume is directly related to the absolute CSF flow ($p = 0.001$) and regurgitant fraction ($p = 0.017$), but the relationship between total

brain CSF volume and net CSF flow was inconclusive ($p = 0.20$). Together, these results suggest that the total CSF volume may impact some of the observations in this study. Further, we investigated whether brain atrophy and aqueductal size impact the CSF flow calculations performed in this study. First, we found that the cross-sectional area of the aqueduct of Sylvius is not significantly affected by age ($p = 0.143$) and that the area of the aqueduct has an inconclusive effect on the maximum ($p = 0.193$) and minimum ($p = 0.487$) CSF flow velocities through the aqueduct. We also observed that total intracranial tissue volume (gray matter plus white matter volumes) has an inconclusive effect on the net CSF flow ($p = 0.382$), absolute CSF flow ($p = 0.428$), and regurgitant fraction metrics ($p = 0.779$). Together, these results suggest that brain atrophy is not a significant factor driving the CSF flow calculations. Another concern with the phase contrast acquisition is the inherent noise in the phase data. During reconstruction, a local phase correction was applied to reduce the effect of eddy currents and concomitant gradients on the phase data.

These findings provide a framework for quantifying aspects of the CSF circulation network and how aging affects this system. These results suggest that ChP hypertrophy may be a compensatory mechanism to maintain adequate CSF production and flow through the aqueduct, but the observation that the net CSF flow decreases with advancing age suggests that this mechanism is inadequate. As the evolving concept of the glymphatic system is further defined, clarifying how CSF production varies across the adult lifespan and in the setting of proteinopathies such as Alzheimer's disease and Parkinson's disease may shed light on the mechanism of CNS waste clearance dysfunction. Work from Hett et al. focused on quantifying more distal components of the brain's waste clearance system in the parasagittal dural space (PSD), finding that PSD volume increased with age and maximum bidirectional CSF flow through the aqueduct.[41] It is important to note the opposite CSF flow sign convention used between Hett and colleagues and this study. Future work should focus on developing noninvasive methods and post-processing techniques to accurately visualize and quantify remaining components of the brain's waste clearance system. For instance, further developments in diffusion tensor imaging may help to quantify glymphatic flow along perivascular spaces,[42] and developments in noninvasive MRI lymphangiography methods[43] may assist in further characterizing waste clearance via the cervical lymphatic vessels.

There were limitations to this study and its analyses. While we aimed to keep the sample age and sex balanced, there were slightly more females than males. However, given that the cohort was approximately matched for age and the significance of the age effect, we do not believe this is a major confound. Second, the predominant race in our sample was white, and the study was not powered to study the effect of race or ethnicity. Third, our CSF flow measurement, as is convention, was not respiratory calibrated. However, we acquired data for five minutes under the assumption that physiological effects from respiration will not contribute significantly over the course of the CSF flow measurement, but it is possible that data integrity could be improved with respiratory correction.[12] Last, small errors in registration of the pCASL images to the T_1-weighted images may lead to some registration inaccuracies. To address this limitation, registered pCASL images were inspected by a board-certified radiologist (CDM) to ensure that the registration to T_1-space was visually correct.

In conclusion, we applied noninvasive magnetic resonance imaging and a novel deep learning algorithm to quantify ChP volume, ChP perfusion, ChP total blood flow, and CSF flow through the aqueduct of Sylvius in a large cohort of healthy adults across the lifespan. Regression analyses provided support for a significant effect of age on all metrics, suggesting that as the ChP hypertrophies, ChP perfusion decreases and CSF flow becomes more regurgitant. Further, we observed that ChP perfusion increases with net CSF flow through the aqueduct in healthy adults, suggesting that ChP perfusion broadly reflects net CSF flow in healthy adults. Values recorded across the lifespan may serve as an exemplar for future studies in the setting of neurodegeneration or cerebrovascular disease where CSF production and flow may be impaired.

Funding

The author(s) disclosed receipt of the following financial support for the research, authorship, and/or publication of this article: This study was funded by NIH/NIA grant 5R01AG062574, NIH/NINR grant 5R01NR015079, and NIH/NCCIH grant 1R01AT011456 and was approved by the Vanderbilt University Medical Center Institutional Review Board.

Availability of data and materials

The data that support the findings of this study are available from the corresponding author, MJD, upon reasonable request.

Declaration of conflicting interests

The author(s) declared the following potential conflicts of interest with respect to the research, authorship, and/or publication of this article: MJD receives research related support from Philips North America; is a paid consultant for Pfizer Inc, Alterity, Global Blood Therapeutics, Graphite Bio, and LymphaTouch; is a paid advisory board member for

Novartis and bluebird bio; receives research funding from Pfizer Inc; and is the President/CEO of Biosight, LLC which operates as a clinical research organization.

Authors' contributions

Authors JJE, CDM, KH, DOC, and MJD contributed to the study design and interpretation of the results. Authors JJE, JE, AKS, AJS, and MJD contributed to the data acquisition. Author CDM contributed to the review of the data. Authors JJE, KH, and MJD contributed to the analysis of the data. All authors contributed to the writing of the manuscript.

ORCID iD

Jarrod J Eisma https://orcid.org/0000-0002-2056-5469

Supplemental material

Supplemental material for this article is available online.

References

1. Brinker T, Stopa E, Morrison J, et al. A new look at cerebrospinal fluid circulation. *Fluids Barriers CNS* 2014; 11: 10–16.
2. Khasawneh AH, Garling RJ and Harris CA. Cerebrospinal fluid circulation: what do we know and how do we know it? *Brain Circ* 2018; 4: 14–18.
3. Cushing H. Studies on the cerebro-spinal fluid: I. Introduction. *J Med Res* 1914; 31: 1–19.
4. Iliff JJ, Wang M, Liao Y, et al. A paravascular pathway facilitates CSF flow through the brain parenchyma and the clearance of interstitial solutes, including amyloid β. *Sci Transl Med* 2012; 4: 147ra111.
5. Johnson SE, McKnight CD, Lants SK, et al. Choroid plexus perfusion and intracranial cerebrospinal fluid changes after angiogenesis. *J Cereb Blood Flow Metab* 2020; 40: 1658–1671.
6. Zhao L, Taso M, Dai W, et al. Non-invasive measurement of choroid plexus apparent blood flow with arterial spin labeling. *Fluids Barriers CNS* 2020; 17: 1–11.
7. Perera C, Harrison IF, Lythgoe MF, et al. Pharmacological MRI with simultaneous measurement of cerebral perfusion and blood-cerebrospinal fluid barrier function using interleaved echo-time arterial spin labelling. *Neuroimage* 2021; 238: 118270.
8. Asllani I, Borogovac A and Brown TR. Regression algorithm correcting for partial volume effects in arterial spin labeling MRI. *Magn Reson Med* 2008; 60: 1362–1371.
9. Zhao L, Feng X, Meyer CH, et al. Choroid plexus segmentation using optimized 3D U-Net. In: *IEEE 17th international symposium on biomedical imaging*. Iowa City, Iowa, USA, 3 April–7 April 2020, pp.381–384. New Jersey: IEEE.
10. Alisch JSR, Kiely M, Triebswetter C, et al. Characterization of age-related differences in the human choroid plexus volume, microstructural integrity, and blood perfusion using multiparameter magnetic resonance imaging. *Front Aging Neurosci* 2021; 13: 734992.
11. Yamada S, Tsuchiya K, Bradley WG, et al. Current and emerging MR imaging techniques for the diagnosis and management of CSF flow disorders: a review of phase-contrast and time–spatial labeling inversion pulse. *AJNR Am J Neuroradiol* 2015; 36: 623–630.
12. Spijkerman JM, Geurts LJ, Siero JCW, et al. Phase contrast MRI measurements of net cerebrospinal fluid flow through the cerebral aqueduct are confounded by respiration. *J Magn Reson Imaging* 2019; 49: 433–444.
13. Nilsson C, Stahlberg F, Thomsen C, et al. Circadian variation in human cerebrospinal fluid production measured by magnetic resonance imaging. *Am J Physiol* 1992; 262: R20–R24.
14. Najafi A, Sartoretti TDJ, Binkert CA, et al. CSF flow quantification in the cerebral aqueduct using phase contrast MR – how to do it properly. In: *ESR European Congress of Radiology, Vienna, Austria*, 28 February–4 March 2018. Austria: ESR.
15. Fonov VS, Evans AC, McKinstry RC, et al. Unbiased nonlinear average age-appropriate brain templates from birth to adulthood. In: *Organization for human brain mapping annual meeting*, San Francisco, California, July 2009, pp.S102. Minnesota: OHBM.
16. Avants BB, Tustison NJ, Song G, et al. A reproducible evaluation of ANTs similarity metric performance in brain image registration. *Neuroimage* 2011; 54: 2033–2044.
17. Çiçek O, Abdulkadir A, Lienkamp SS, et al. 3D U-Net. Learning dense volumetric segmentation from sparse annotation. In: *International conference on medical image computing and computer-assisted intervention*, Athens, Greece, 17 October–21 October 2016, pp.424–432. Minnesota: MICCAI.
18. Liu TT and Wong EC. A signal processing model for arterial spin labeling functional MRI. *Neuroimage* 2005; 24: 207–215.
19. Alsop DC, Detre JA, Golay X, et al. Recommended implementation of arterial spin-labeled perfusion MRI for clinical applications: a consensus of the ISMRM perfusion study group and the European Consortium for ASL in dementia. *Magn Reson Med* 2015; 73: 102–116.
20. Brown RW, Cheng YCN, Haacke EM, et al. *Magnetic resonance imaging: physical principles and sequence design*. 1st ed. New York: Wiley-Liss, 1999, p.727.
21. R Core Team 2014. R: a language and environment for statistical computing. *R foundation for statistical computing*. Vienna, Austria: Author.
22. Benjamini Y and Hochberg Y. Controlling the false discovery rate: a practical and powerful approach to multiple testing. *J R Stat Soc Ser B* 1995; 57: 289–300.
23. Shapiro SS and Wilk MB. An analysis of variance test for normality (complete samples). *Biometrika* 1965; 52: 591–611.
24. Serot JM, Foliguet B, Béné MC, et al. Choroid plexus and ageing in rats: a morphometric and ultrastructural study. *Eur J Neurosci* 2001; 14: 794–798.
25. Sturrock RR. An ultrastructural study of the choroid plexus of aged mice. *Anat Anz* 1988; 165: 379–385.

26. Serot JM, Béné MC, Foliguet B, et al. Morphological alterations of the choroid plexus in late-onset Alzheimer's disease. *Acta Neuropathol* 2000; 99: 105–108.
27. Serot JM, Béné MC and Faure GC. Choroid plexus, aging of the brain, and Alzheimer's disease. *Front Biosci* 2003; 8: s515–s521.
28. Shuangshoti S and Netsky MG. Human choroid plexus: morphologic and histochemical alterations with age. *Am J Anat* 1970; 128: 73–95.
29. Ferrante F and Amenta F. Enzyme histochemistry of the choroid plexus in old rats. *Mech Ageing Dev* 1987; 41: 65–72.
30. Cottrell DA, Blakely EL, Johnson MA, et al. Cytochrome oxidase deficient cells accumulate in the hippocampus and choroid plexus with age. *Neurobiol Aging* 2001; 22: 265–272.
31. Kvitnitskaia-Ryzhova TI and Shkapenko AL. A comparative ultracytochemical and biochemical study of the ATPases of the choroid plexus in aging. *Tsitologiia* 1992; 34: 81–87.
32. Preston JE. Age-related reduction in rat choroid plexus chloride efflux and CSF secretion rate. In: *Society for neuroscience*, Miami, Florida, USA, 23 October–28 October 1999, pp.697–698. Washington, DC: SfN.
33. Chen RL, Kassem NA, Redzic ZB, et al. Age-related changes in choroid plexus and blood-cerebrospinal fluid barrier function in the sheep. *Exp Gerontol* 2009; 44: 289–296.
34. May C, Kaye JA, Atack JR, et al. Cerebrospinal fluid production is reduced in healthy aging. *Neurology* 1990; 40: 500–503.
35. Sartoretti T, Wyss M, Sartoretti E, et al. Sex and age dependencies of aqueductal cerebrospinal fluid dynamics parameters in healthy subjects. *Front Aging Neurosci* 2019; 11: 199.
36. Gideon P, Thomsen C, Ståhlberg F, et al. Cerebrospinal fluid production and dynamics in normal aging: a MRI phase-mapping study. *Acta Neurol Scand* 1994; 89: 362–366.
37. Stoquart-Elsankari S, Balédent O, Gondry-Jouet C, et al. Aging effects on cerebral blood and cerebrospinal fluid flows. *J Cereb Blood Flow Metab* 2007; 27: 1563–1572.
38. Barkhof F, Kouwenhoven M, Scheltens P, et al. Phase-contrast cine MR imaging of normal aqueductal CSF flow: effect of aging and relation to CSF void on modulus MR. *Acta Radiol* 1994; 35: 123–130.
39. Wilson MR, Preston JE, Thomas SA, et al. Altered cerebrospinal fluid secretion rate and 125I-labelled β-amyloid transport in the aged sheep isolated perfused choroid plexus. *J Physiol* 1999; 515: 7–8.
40. Pollay M and Curl F. Secretion of cerebrospinal fluid by the ventricular ependyma of the rabbit. *Am J Physiol* 1967; 213: 1031–1038.
41. Hett K, McKnight CD, Eisma JJ, et al. Parasagittal dural space and cerebrospinal fluid (CSF) flow across the lifespan in healthy adults. *Fluids Barriers CNS* 2022; 19: 24.
42. Taoka T, Masutani Y, Kawai H, et al. Evaluation of glymphatic system activity with the diffusion MR technique: diffusion tensor image analysis along the perivascular space (DTI-ALPS) in Alzheimer's disease cases. *Jpn J Radiol* 2017; 35: 172–178.
43. Crescenzi R, Donahue PMC, Hartley KG, et al. Lymphedema evaluation using noninvasive 3T MR lymphangiography. *J Magn Reson Imaging* 2017; 46: 1349–1360.